

**Ion temperature effects on plasma flow in the magnetic mirror configuration**A. Sabo,<sup>1</sup> A. I. Smolyakov,<sup>1</sup> P. Yushmanov,<sup>2</sup> and S. Putvinskii<sup>2</sup><sup>1)</sup> *University of Saskatchewan, Saskatchewan, Saskatoon SK S7N 5E2, Canada*<sup>2)</sup> *TAE Technologies, 19631 Pauling, Foothill Ranch, CA, 92610, United States*

Effects of finite ion temperature on plasma flow in the converging-diverging magnetic field, the magnetic mirror, or equivalently, magnetic nozzle configuration, are studied using a quasineutral paraxial two-fluid MHD model with isothermal electrons and magnetized ions. The magnetized ions are considered in the two-pressure approximation with Chow-Golberger-Law model and its generalization. The solutions of stationary MHD equations were studied with an emphasis on the role of the singularity at the sonic point transition. It is shown that the regularity of the sonic point defines a global solution describing plasma acceleration from subsonic to supersonic velocity. Such stationary solutions were compared with the time dependent dynamics confirming that the solutions of the time-dependent equations converge to the stationary solutions. It is shown that the perpendicular ion pressure enhances plasma acceleration due to the mirror force. The role of ion dissipative effects such as ionization and charge exchange on plasma flow acceleration have been investigated.

Keywords: Plasma acceleration, magnetic nozzle, anisotropic pressure, CGL, mirror machine

## I. INTRODUCTION

The plasma flow in the magnetic mirror configuration (magnetic nozzle) plays an important role in a number of devices, such as magnetic mirrors used in fusion research and devices for electric propulsion in space. In plasma propulsion, magnetic nozzle configuration is employed to convert the plasma thermal energy into the ion kinetic energy, thus generating thrust<sup>1,2</sup>. In open mirror fusion devices, the expanding magnetic field of the divertor (expander region) is used to spread the energy over the larger area to reduce the wall heat loads<sup>3</sup>. Plasma flow in the edge region of the divertor tokamak also experiences acceleration to supersonic velocities due to the combined effects of plasma pressure and inhomogeneous magnetic field<sup>4-6</sup>. Various aspects of plasma flow and acceleration in the magnetic mirror configurations have been studied. General framework of plasma flow and acceleration in the MHD approximation was formulated in Ref. 7, and subsequently used to study plasma detachment<sup>8</sup>, acceleration mechanisms and propulsion efficiency<sup>9,10</sup>. The role of the magnetic nozzle in the conversion of plasma thermal energy to supersonic flow was demonstrated experimentally<sup>11,12</sup>. The MHD models were used to study the supersonic acceleration in scrape-off-layer (SOL) of tokamak edge in Refs. 13–15. Ion pressure anisotropy was considered and related mirror force effects on the plasma flow in the SOL were observed in Refs. 14 and 15, and the predictions of the isotropic and anisotropic pressure models were compared.

It is well known that in the quasineutral approximation the ion inertia and finite temperature result in the appearance of the sonic point singularity at the point where the local ion velocity is equal to the ion sound speed  $c_s$ . It has recently been emphasized<sup>16</sup> that the conditions at the sonic point in the nozzle region where the magnetic field has the maximum are critical for the existence of the smooth accelerating solution such that the resulting plasma flow is uniquely defined in the whole converging-diverging region, i.e. in the whole range from sub-sonic,  $V < c_s$ , to super-sonic,  $V > c_s$ , velocities. In this paper we study the role of finite ion temperature and dissipation due to ionization and charge-exchange on plasma flow and acceleration in the context of the magnetic fusion experiments<sup>3,15</sup>. These results are also of interest for propulsion devices where a large ion temperature is expected, such as in VASIMR<sup>2</sup>. We specifically analyze the role of the sonic point singularity on the properties of the stationary flow solution. In this paper we investigate the modifications of the sonic

point and the acceleration due to the ion pressure anisotropy as well as the ionization and charge-exchange processes that affect the ion pressure evolution.

The basic model equations are presented in Section II. The Section III discusses general features of the sonic point singularity and ion acceleration with finite ion pressure. Plasma acceleration for cold ions is reviewed in Section IV. The Section V presents the results of the solution of the stationary and dynamic (time-dependent) equations for the base case with anisotropic pressure. The Section VI analyzes modifications due to the ionization and charge-exchange collisions. The summary and discussions are presented in the Section VII.

## II. BASIC MODEL

Our basic model consist of the massless electron momentum equation in the isothermal  $T_e = const$  approximation, the ion momentum, continuity and ion pressure evolution equations for warm ions which are described by the two-pressure Chow-Goldberger-Law (CGL) model<sup>17</sup> in the form

$$\frac{d}{dt} \left( \frac{p_{\parallel} B^2}{n^3} \right) = S_{\parallel}, \quad (1)$$

$$\frac{d}{dt} \left( \frac{p_{\perp}}{nB} \right) = S_{\perp}. \quad (2)$$

We consider a problem in the paraxial approximation so that the total fluid time derivative for ions is  $d/dt = \partial/\partial t + V_{\parallel} \nabla_{\parallel}$ , where  $V_{\parallel} = \mathbf{V} \cdot \mathbf{B}/B$  is the ion parallel velocity,  $\nabla_{\parallel} = \mathbf{B} \cdot \nabla/B$ , and  $\mathbf{b} = \mathbf{B}/B$  represents a unit vector in the direction of the magnetic field.

In the context of the plasma flow and acceleration along the open magnetic field lines the anisotropic MHD equations were considered in Refs. 18 and 19. Similar equations also follow from the drift-kinetic<sup>20</sup> or gyro-fluid equations<sup>21,22</sup> in the appropriate limit. The fluid models implemented in the simulations of plasma flow in the SOL tokamak regions include additional source/sink terms in the density, momentum, and energy equations as well as some approximations for the heat fluxes and relaxation terms<sup>15</sup>. In this paper, our emphasis is on the ion pressure effects, so we use the standard adiabatic CGL equations<sup>17</sup> modified with the model sink terms  $S_{\parallel}$  and  $S_{\perp}$  to model the effects of ionization and charge-exchange on the ion pressure evolution, cf. Eqs. (1) and (2). In general, ionization contribute to the density, ion momentum as well as pressure evolution, while the charge exchange affects the ions momentum and pressure evolution. The ionization coefficients depend on the neutral

species, their density and electron temperature and electron density, while charge-exchange coefficients depend on the ions/neutral density and their energy. Thus the ionization and charge-exchange effects may have complex profile dependencies depending on the particular situation and plasma parameters. In this study we are interested in the main parametric trends due to the ionization and charge exchange. Thus, we use a simplified model where the effects of ionization and charge exchange are represented by two constant coefficients  $\nu_1$  and  $\nu_2$ . The  $\nu_1$  coefficient corresponds to the ionization, while the  $\nu_2$  coefficient in the ion momentum equation describes the total effects of ionization and charge-exchange. In this study we neglect the heat flux effects in the energy (pressure evolution) as well as any possible ionization heating terms<sup>23</sup> and only the pressure "decay" terms are included with the same coefficient  $\nu_2$  for  $p_{\parallel}$  and  $p_{\perp}$ . In the expanded form, the full systems of equations including the ionization and charge-exchange effects is then written in the form similarly to Ref.3:

$$\frac{\partial n}{\partial t} = nV_{\parallel} \frac{\partial \ln B}{\partial z} - V_{\parallel} \frac{\partial n}{\partial z} - n \frac{\partial V_{\parallel}}{\partial z} + \nu_1 n, \quad (3)$$

$$m_i n \left( \frac{\partial V_{\parallel}}{\partial t} + V_{\parallel} \frac{\partial V_{\parallel}}{\partial z} \right) = -en \frac{\partial \phi}{\partial z} - \frac{\partial p_{\parallel}}{\partial z} + (p_{\parallel} - p_{\perp}) \times \frac{\partial \ln B}{\partial z} - \nu_2 m_i n V_{\parallel}, \quad (4)$$

$$\frac{\partial p_{\parallel}}{\partial t} = p_{\parallel} V_{\parallel} \frac{\partial \ln B}{\partial z} - V_{\parallel} \frac{\partial p_{\parallel}}{\partial z} - 3p_{\parallel} \frac{\partial V_{\parallel}}{\partial z} - \nu_2 p_{\parallel}, \quad (5)$$

$$\frac{\partial p_{\perp}}{\partial t} = 2p_{\perp} V_{\parallel} \frac{\partial \ln B}{\partial z} - V_{\parallel} \frac{\partial p_{\perp}}{\partial z} - p_{\perp} \frac{\partial p_{\perp}}{\partial z} - \nu_2 p_{\perp}. \quad (6)$$

The electrons are assumed in the Boltzmann form with constant uniform temperature

$$0 = en \frac{\partial \phi}{\partial z} - T_e \frac{\partial n}{\partial z}. \quad (7)$$

We have to note that additional terms represented by the  $nu_1$  and  $\nu_2$  in coefficients in the continuity, momentum, and pressure equations are model approximations aiming to describe the effects of ionization and charge-exchange on the *plasma acceleration and flow* in the region of the magnetic mirror and external expander regions, denoted as  $0 < z < L$ . Here we do not consider the main plasma source region  $z < 0$ .

Before we proceed with the general case, we consider general conditions for the existence of accelerating solutions and simplified cases of cold and warm ions in absence of ionization and charge-exchange effects.

### III. THE SONIC POINT SINGULARITY AND PLASMA ACCELERATION

In this section we consider a general condition for the existence of the global stationary accelerating solution in the absence of ionization and charge-exchange. Setting  $\nu_1 = \nu_2 = 0$ , one can obtain from (7 - 6) the following equation for the ion velocity

$$\left( M^2 - 1 - \frac{3p_{\parallel}}{nT_e} \right) \frac{\partial M}{\partial z} = - \left( 1 + \frac{p_{\perp}}{nT_e} \right) M \frac{\partial \ln B}{\partial z}. \quad (8)$$

Here  $M = V_{\parallel}/c_s$  is the plasma velocity  $V_{\parallel}$  normalized to the speed of sound  $c_s = \sqrt{(T_e/m_i)}$ .

Equation (8) describes ion acceleration with finite anisotropic pressure. This equation has to be solved simultaneously with equations (5) and (6) for  $p_{\perp}$  and  $p_{\parallel}$ . The acceleration is provided by the electron pressure and is enhanced by the ion transverse pressure, due to the mirror force. Equation (8) demonstrates a singularity at the sonic point which in our case is modified by the parallel ion pressure effect,  $M = M_{cr} = \sqrt{1 + 3p_{\parallel}/nT_e}$ . Generally supersonic acceleration in the magnetic mirror configuration is similar to the Laval nozzle acceleration. For the low velocity  $M < M_{cr}$ , the acceleration occurs due to the effective area cross-section decrease due to the magnetic field rise,  $\partial \ln B / \partial z > 0$ . After the critical point  $M > M_{cr}$ , in the region of decreasing magnetic field with  $\partial \ln B / \partial z < 0$  the acceleration continues supported by the electric field generated by the electron and ion pressure. Two accelerating regions can be matched and global smooth accelerating solution can only be obtained by regularizing the sonic point at the point  $z = z_m$  where  $\partial \ln B / \partial z = 0$ , which therefore requires the condition

$$\left| M^2 - 1 - \frac{3p_{\parallel}}{nT_e} \right|_{z=z_m} = 0. \quad (9)$$

Expanding the left and right sides of (8) near the singular point and using equation (9) one obtains the expression for the  $\partial M / \partial z$  derivative near  $z = z_m$  :

$$\begin{aligned} \left( \frac{\partial M}{\partial z} \right)^2 &= - \frac{(1 + p_{\perp}/nT_e)(1 + 3p_{\parallel}/nT_e)}{2(1 + 6p_{\parallel}/nT_e)} \frac{\partial^2 \ln B}{\partial z^2} \Big|_{z=z_m} \\ &= - \frac{(1 + T_{\perp}/T_e)(1 + 3T_{\parallel}/T_e)}{2(1 + 6T_{\parallel}/T_e)} \frac{\partial^2 \ln B}{\partial z^2} \Big|_{z=z_m}. \end{aligned} \quad (10)$$

This expression illustrates that the condition  $\partial^2 \ln B / \partial z^2 < 0$ , i.e. maximum of the magnetic field, for  $z = z_m$ , is required for the existence of a smooth (regular) solution.

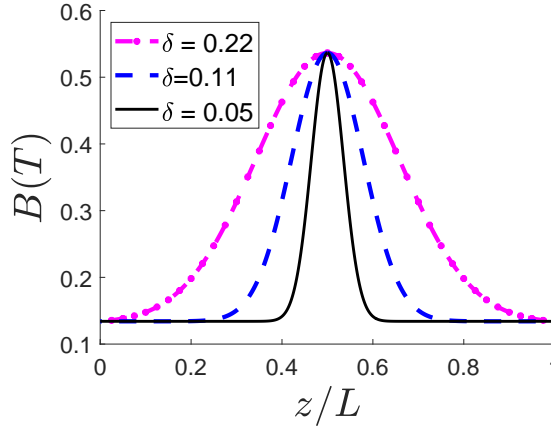


FIG. 1. Different magnetic field profiles with the mirror ratio  $R=4$  at  $z = 0$  and  $z = L$ .

#### IV. THE ACCELERATING POTENTIAL FOR THE CASE OF COLD IONS

The case of cold ions provides a simple illustration of the properties of the accelerating potential formed by the converging-diverging magnetic field configuration. For  $p_{\perp} = p_{\parallel} = 0$ , Eq.(8) can be integrated<sup>24–26</sup> resulting in the implicit equation for the ion velocity in the form

$$\frac{M^2}{2} - \frac{1}{2} = -\ln \left( \frac{B(z)}{M(z) B_m} \right). \quad (11)$$

Here  $B_m = B(z)$  at  $z = z_m$  and the integration constant was chosen so the solution is regular at  $z = z_m$ , and the derivative  $\partial M / \partial z$  is fixed to

$$\left( \frac{\partial M}{\partial z} \right)^2 = - \frac{1}{2} \frac{\partial^2 \ln B}{\partial z^2} \Big|_{z=z_m}. \quad (12)$$

The exact solution for equation (11) was presented in Ref. 16 in terms of the Lambert function which appears in various plasma physics problems<sup>27,28</sup>. Here, for illustration, we consider the magnetic field mirror with Gaussian profile,  $B(z) = (B_m - B_0) \exp(-(z - z_0)^2 / (\delta^2 L^2)) + B_0$ , giving a mirror ratio  $R = B_m / B(z) = 4$  at both ends,  $z = 0$  and  $z = L$ . Several cases with different width were considered changing  $\delta$ , as shown in Fig. 1. Also different values of the mirror ratio were considered by changing the value  $B_0$ . Equation (11) shows that the local value of the plasma velocity is defined by the local value of the magnetic field. This solution has a global character defined by the regularization condition at the sonic point,  $V_{\parallel} = c_s$ . For cold plasma, the sonic point is at  $\frac{\partial \ln B}{\partial z} = 0$ , and the condition for the regular (smooth) solution defines the velocity derivative at this point, therefore fixing the velocity

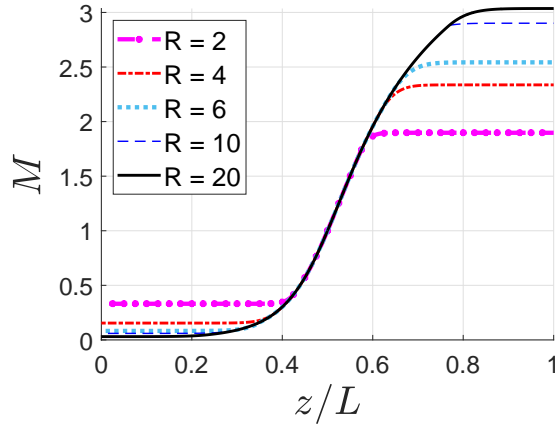


FIG. 2. Plasma velocity profiles for different values of the mirror ratio.

profile globally. Note that plasma density  $n$  scales out from the solution for the velocity, and can be defined from the value of the flux at  $z = z_m$  from the flux conservation

$$\frac{n(z)V_{\parallel}(z)}{B(z)} = \frac{n_0V_{\parallel 0}}{B_0}. \quad (13)$$

Therefore, the profile of the density is defined by the magnetic field and velocity profiles but the relative amplitude of density can be normalized by the condition at  $z = 0$ . The equation (10) shows that the sub-sonic acceleration,  $M(z) < 1$ , is mostly due to the effective area decrease, while in the super-sonic regime,  $M(z) > 1$ , the acceleration is driven by the electric field due to the electron pressure. The velocity, density, and potential profiles for different values of  $\delta$  are shown in the following figures (3), (4), and (5).

Increase of the mirror ratio leads to the decrease of the initial velocity  $M_0 = M(0) < 1$ , and increase of the final velocity at  $z = L$ ,  $M(L) > 1$ . The final velocity only depends on the mirror ratio  $R$  (regardless of the the details of the magnetic field profile), and has weak logarithmic divergence for  $R \gg 1$ , as is shown in Fig. 2.

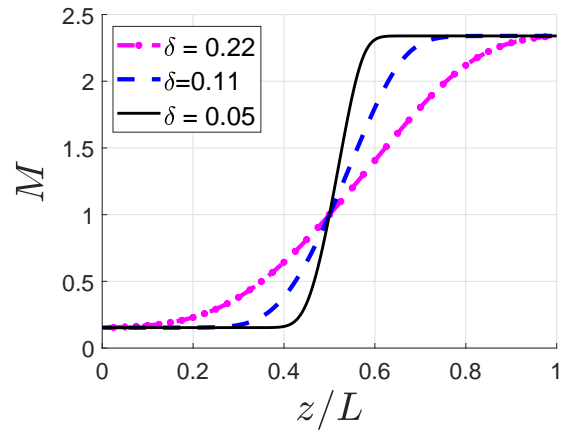


FIG. 3. Plasma velocity for different magnetic field profiles.

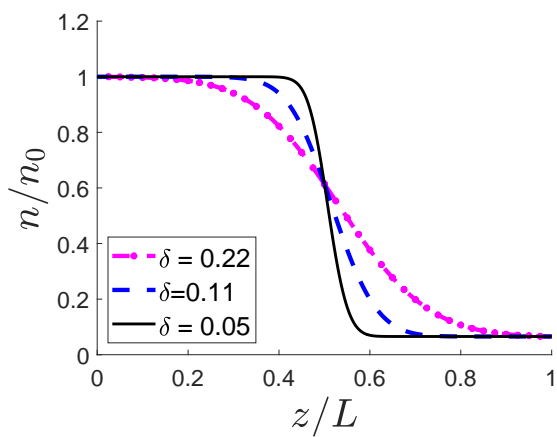


FIG. 4. Plasma density for different magnetic field profiles.

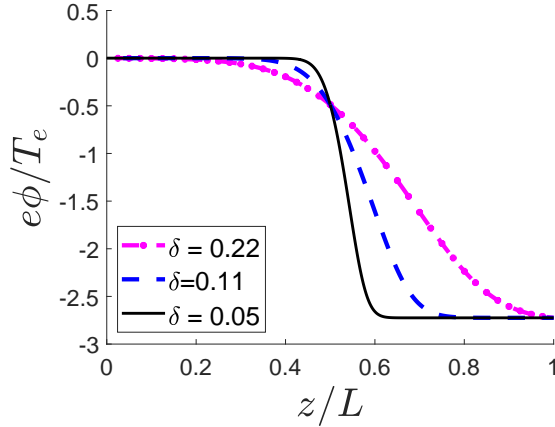


FIG. 5. Electrostatic potential for different magnetic field profiles

## V. EFFECT OF THE FINITE ION TEMPERATURE ON PLASMA FLOW

In this Section, we present the global regular solution for plasma flow from the plasma source at  $z < 0$  with the magnetic field profile similar to one in the C-2U device<sup>3,29</sup> shown in Fig. 6. The global solutions are considered in the region  $0 < z < L$ . The mirror ratios were  $B_m/B_0 = 8.0$  and  $B_m/B_r = 20.0$  at the left,  $z = 0$ , and the right,  $z = L$ , ends of the nozzle, respectively. The magnetic field setup is described in more detail in the Appendix. The left side of the simulation region represents the transition to the plasma source at  $z < 0$ . We assume that the ion plasma pressure is isotropic at this point,  $p_{\perp}(0) = p_{\parallel}(0)$  and plasma density is fixed,  $n = n_0$ . It is important to note that plasma velocity is fixed globally by the condition at the singular point, so that it cannot be taken arbitrary at  $z = 0$ ; the value at the exit point,  $z = L$  is uniquely fixed as well. We will discuss this constraint and its consequences further below. Note that while the profiles of the density and pressure are fully determined by the global solution, the absolute values have free normalization parameters. Here, they are normalized to the values at  $z = 0$ ,  $n_0, p_{\perp 0}, p_{\parallel 0}$ .

The numerical solution of stationary equations (8) and (7 - 6) are obtained by the integration from the the proximity of the sonic point,  $z_m/L = 0.5$ , in both  $z < z_m$  and  $z > z_m$  directions. The initial conditions for the parameters  $M, n, p_{\parallel}$ , and  $p_{\perp}$  are obtained from the Taylor series expansion near  $z = z_m$ . Across the entire nozzle electrons were assumed to be isothermal with  $T_e = 200eV$ . At the left end of the nozzle it was assumed that

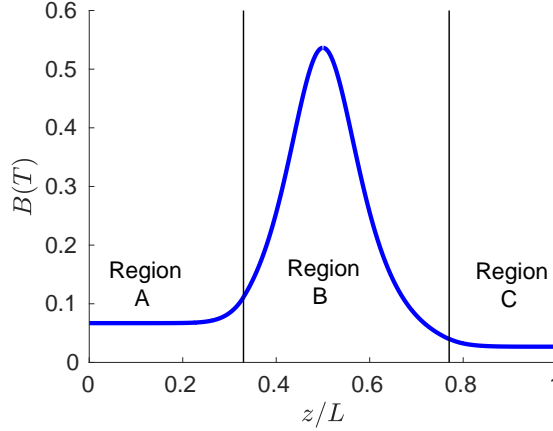


FIG. 6. Magnetic field of the mirror configuration as in Ref.3 and 29

$T_{i\parallel 0} = T_{i\perp 0} = 200\text{eV}$  with the density  $n_0 = 1.0 \times 10^{19}\text{m}^{-3}$ , however all results can be represented in dimensionless units. The shooting method was used to achieve the final solution with isotropic ion pressure,  $T_{i\parallel 0} = T_{i\perp 0} = 200\text{eV}$  at the left end of the nozzle.

Steady-state solutions of stationary equations obtained by the shooting method were compared with the time-dependent solutions obtained as a solution of the initial value problem for equations (3 - 6), presented in the Appendix with additional details. We have verified that the solution of the time-dependent equations converge well to the stationary solution obtained by the different method, the results being displayed in figures (7), (10), (11) and (12). The characteristic time was  $t_c = L/c_s = 1.0 \times 10^{-4}\text{s}$  and each time interval was given as a multiple of  $t_c$ . Each time step in the simulation was equivalent to  $1.0^{-4}t_c$ . The evolution of the time-dependent problem toward the stationary solution is shown in Fig. 8 for the successive moments in time  $t_1 < t_2 \dots < t_5$  with the lowest  $t_1 = 1.0 \times 10^{-2}t_c$  and the stationary solution value being reached at  $t = 1.5t_c$ .

The ion temperatures  $T_{i\parallel} = T_{i\perp} = 200\text{eV}$  were changed to study the effect on plasma flow. Three additional cases were studies with  $T_{i\parallel} = T_{i\perp} = 400\text{eV}$ ,  $T_{i\parallel} = T_{i\perp} = 50\text{eV}$  and compared with the case of cold ions with  $T_{i\parallel} = T_{i\perp} = 0\text{eV}$ , while  $T_e = 200\text{eV}$  remained the same.

Similarly to the case of cold ions, plasma acceleration occurs in the regions with the finite gradient of the magnetic field. The perpendicular ion pressure enhances the ion acceleration

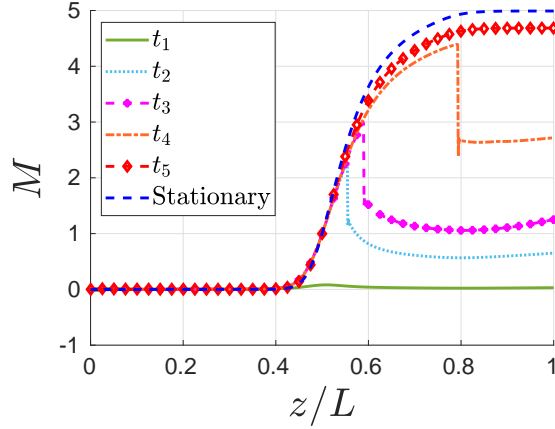


FIG. 8. Time evolution of the velocity profile.

according to equation (10). The parallel ion pressure shifts the sonic point. However, the parallel pressure decreases fast with distance so it effects on the location of the singular point is not significant for our parameters. For the initial isotropic ion pressure state at  $z = 0$ , the finite ion temperatures increases the velocity of the accelerated ions as shown in Fig. 9 and displayed in Table 1.

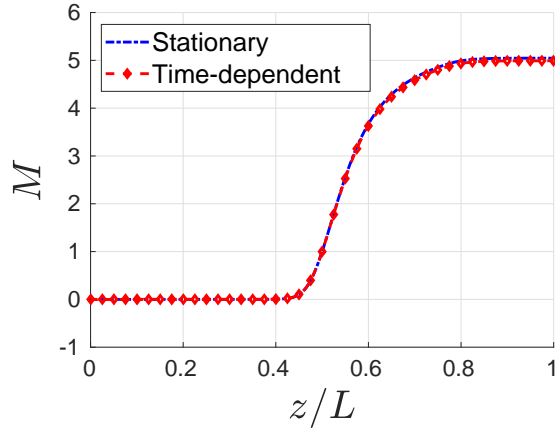


FIG. 7. Comparison of stationary and time-dependent solutions.

An interesting observation that can be seen from Fig. 10 is that for a finite ion temperature there is a region where the density is increasing with distance, contrary to the case of cold ions, where the density is always monotonically decreasing. A similar behavior is observed for the potential, with the small increase with distance being displayed in Fig. 14

$T_{i\parallel 0}(eV)$	$T_{i\perp 0}(eV)$	$M_0$	$M_L$
400	400	$1.326 \times 10^{-6}$	6.4067
200	200	$3.179 \times 10^{-4}$	5.0404
50	50	0.0193	3.6603
0	0	0.0762	3.0388

TABLE I. Plasma Mach number values for different ion temperature at  $z = 0$ .

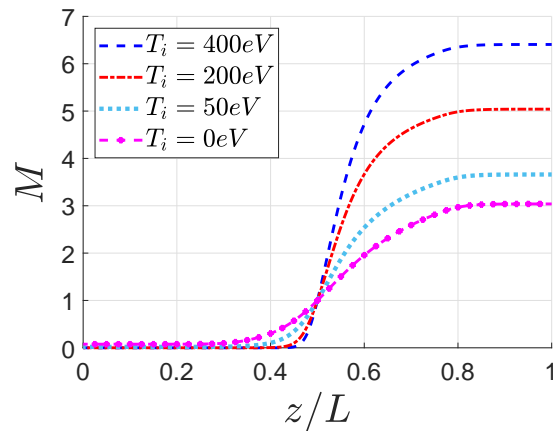


FIG. 9. Mach number  $M$  for different initial ion temperatures

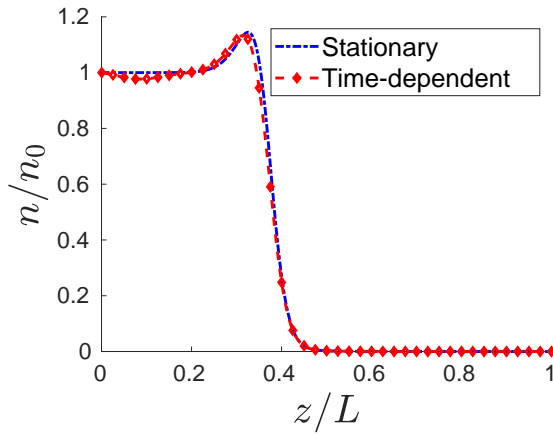


FIG. 10. Stationary and time-dependent solutions of plasma density

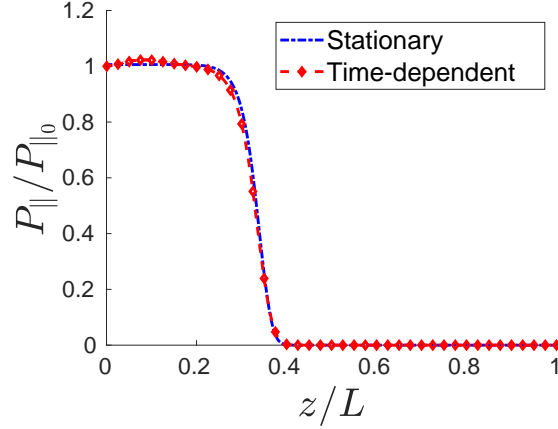


FIG. 11. Parallel plasma pressure

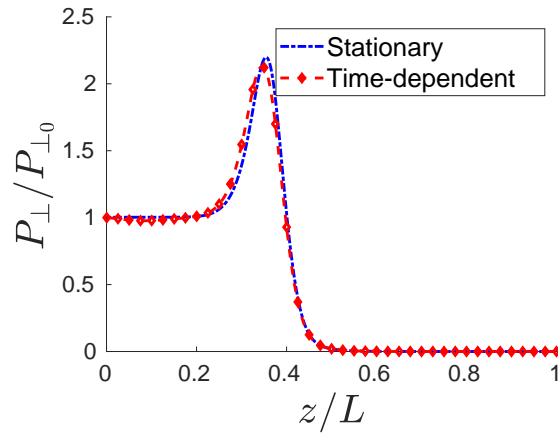


FIG. 12. Perpendicular plasma pressure

The perpendicular plasma pressure follows the increase of the magnetic field  $B$  related to the conservation of the adiabatic invariant, expressed in equation (13), as  $T_{i\perp}(z)/B(z) = \text{const}$ . The dependence of  $T_{i\perp}, T_{i\parallel}$  on  $B(z)$  are shown in Fig. 13. The decrease of  $T_{i\parallel}$  in the outer region is related to strong plasma density dependence  $\sim n^3$  in the CGL equation of state for  $P_{\parallel}$  and density decrease due to plasma acceleration.

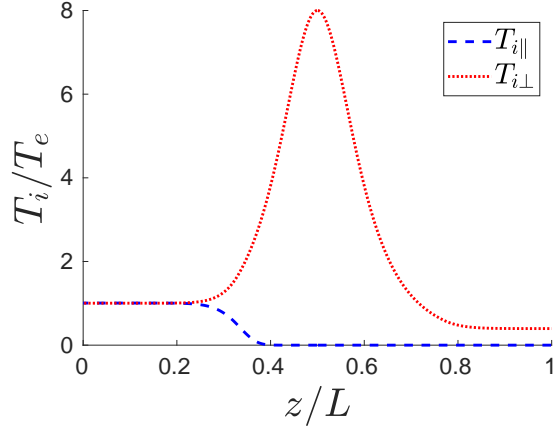


FIG. 13. Parallel and perpendicular ion temperatures

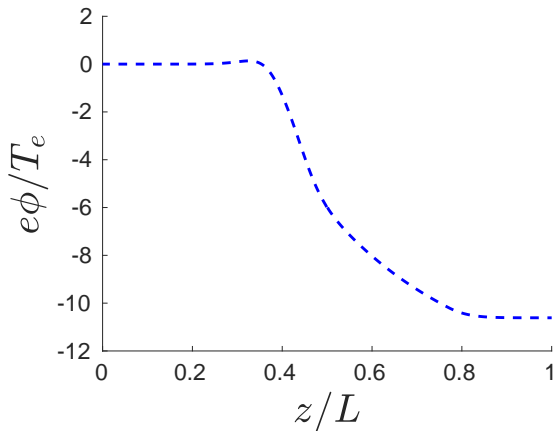


FIG. 14. Electrostatic potential

## VI. IONIZATION AND CHARGE-EXCHANGE EFFECTS

In this section we consider the ion flow taking into account the ionization and charge-exchange effects. These effects are important in fusion applications due to presence of neutrals in the mirror region. Effects of neutrals were also considered in propulsion applications. Depending on the application, neutral density and therefore ionization and charge-exchange rates may vary in a rather wide range<sup>3,30</sup>. To estimate possible effects at various conditions, here we use generic form of the sink terms  $S_{\parallel}$  and  $S_{\perp}$  with various values of  $\nu_1$  and  $\nu_2$  in normalized form  $\nu'_2 = \frac{\nu_2 L}{c_s}$ ,  $\nu'_1 = \frac{\nu_1 L}{c_s}$  from low to large values. These rates are assumed

constant throughout the nozzle. The rest of plasma parameters are normalized to their respective values at the left end of the nozzle such that  $n' = \frac{n}{n_0}$ ,  $p'_{\parallel} = \frac{p_{\parallel}}{p_{\parallel 0}}$ ,  $p'_{\perp} = \frac{p_{\perp}}{p_{\perp 0}}$ ,  $T'_{i\parallel} = \frac{T_{i\parallel}}{T_e}$ ,  $T'_{i\perp} = \frac{T_{i\perp}}{T_e}$ ,  $z' = \frac{z}{L}$  and  $t' = \frac{c_s}{L}t$  where  $L = 4\text{ m}$  is the length of the nozzle. (For the sake of convenience all the primes on parameters will be dropped and it will be assumed that  $n$ ,  $p_{\parallel}$ ,  $p_{\perp}$ ,  $\phi$ ,  $T_{i\parallel}$ ,  $T_{i\perp}$ ,  $T_e$ ,  $z$  and  $t$  represent normalized quantities). In dimensionless form (omitting the primes on normalized variables) the stationary equations describing ion dynamics have the form

$$\frac{\partial n}{\partial z} = n \left( \frac{\partial \ln B}{\partial z} - \frac{1}{M} \frac{\partial M}{\partial z} + \frac{\nu_1}{M} \right), \quad (14)$$

$$\frac{\partial p_{\parallel}}{\partial z} = p_{\parallel} \left( \frac{\partial \ln B}{\partial z} - \frac{3}{M} \frac{\partial M}{\partial z} - \frac{\nu_2}{M} \right), \quad (15)$$

$$\frac{\partial p_{\perp}}{\partial z} = p_{\perp} \left( 2 \frac{\partial \ln B}{\partial z} - \frac{3}{M} \frac{\partial M}{\partial z} - \frac{\nu_2}{M} \right), \quad (16)$$

$$\begin{aligned} \left( M^2 - 1 - \frac{3p_{\parallel}}{nT_e} \right) \frac{\partial M}{\partial z} = & - \left( 1 + \frac{p_{\perp}}{nT_e} \right) M \frac{\partial \ln B}{\partial z} \\ & + \left( \frac{p_{\parallel}}{nT_e} - M^2 \right) \nu_2 - \nu_1, \end{aligned} \quad (17)$$

$$\phi = T_e \ln \left( \frac{n}{n_L} \right). \quad (18)$$

Additional terms in Eq. (17) due to the ionization and charge exchange effects modify the regularization condition at the sonic point. Expanding near this point we obtain for  $\frac{\partial M}{\partial z}$  at the singular point the following equation

$$a \left( \frac{\partial M}{\partial z} \right)^2 + b \left( \frac{\partial M}{\partial z} \right) + c = 0, \quad (19)$$

where

$$a = 2 \left( 1 + \frac{6T_{i\parallel m}}{T_e} \right), \quad (20)$$

$$\begin{aligned} b = & \frac{5T_{i\parallel m}}{T_e} \nu_2 + \frac{3T_{i\parallel m}}{T_e} \nu_1 + \left( 1 + \frac{T_{i\perp m}}{T_e} \right) \left( 1 + \frac{3T_{i\parallel m}}{T_e} \right)^{\frac{1}{2}} \\ & \times \frac{\partial \ln B}{\partial z} + 2 \left( 1 + \frac{3T_{i\parallel m}}{T_e} \right) \nu_2, \end{aligned} \quad (21)$$

$$\begin{aligned}
c = & \left(1 + \frac{T_{i\perp m}}{T_e}\right) \left(1 + \frac{3T_{i\parallel m}}{T_e}\right) \frac{\partial^2 \ln B}{\partial z^2} + \frac{T_{i\perp m}}{T_e} \\
& \times \left(1 + \frac{3T_{i\parallel m}}{T_e}\right) \left(\frac{\partial \ln B}{\partial z}\right)^2 - \frac{T_{i\perp m}}{T_e} \left(1 + \frac{3T_{i\parallel m}}{T_e}\right)^{\frac{1}{2}} \\
& \times \frac{\partial \ln B}{\partial z} (\nu_2 + \nu_1) + \frac{T_{i\parallel m}}{T_e} (\nu_2 + \nu_1) \nu_2.
\end{aligned} \tag{22}$$

Here  $T_{i\parallel m}$  and  $T_{i\perp m}$  are the values of the parallel and perpendicular temperature at the sonic point, which no longer occurs at  $z = z_m$  but is shifted to the right. The shift in the location of the sonic point depends on the values of  $\nu_1$  and  $\nu_2$  with higher values shifting the sonic point further away from its initial position at  $z = z_m$ . Similar to Section III, we obtain stationary solutions for equations (14) - (18) using the shooting method as described in Section II and compare these solutions with the solution of the initial value problem given by equations (7) - (6). Again, it has been confirmed that time-dependent solutions converge well to the stationary solutions after some relaxation.

There are several features introduced by ionization and charge-exchange effects. One is a non-monotonous behavior of plasma density with the increase due to the ionization, which is especially noticeable in the region of flat magnetic field before any substantial acceleration occurs. Related to the density behavior, the potential also shows a non-monotonous increase in the region to the left of the maximum of the magnetic field as shown in Fig. 19.

Another effect introduced by the dissipative terms, is the modification of the perpendicular pressure profile so that it does not follow the increase in the magnetic field. The latter effect is much reduced by dissipation so the perpendicular pressure profile may become similar to the parallel pressure with almost monotonous decrease throughout the whole region, and both the parallel and perpendicular pressure having very similar profiles with  $T_{i\parallel}$  and  $T_{i\perp}$  as displayed in Figures 17 and 18. With the above noted modifications, the resulting velocity has a significantly larger value at the at the left boundary,  $M = 0.127$ , compared with the case in absence of charge-exchange and ionization, and a lower final acceleration value on the exit side of the nozzle. One has to note also that the presence of the dissipative terms due to the ionization and charge-exchange results in the shift of the position of the sonic point so it is no longer at the magnetic field maximum, as described by equation (19).

The effect of charge-exchange has been further studied for various values of  $\nu_2$  as shown in Table II and Figures 15, 16, 17, 18 and 19. Further increase in  $\nu_2$  results in the non-

$\nu_2$	$M_0$	$M_L$	$e\phi/T_{e0}$	$e\phi/T_{eL}$
0	$3.179 \times 10^{-4}$	5.045	0	-10.613
0.1	0.0311	3.576	0	-5.542
0.35	0.073	3.152	0	-4.63
1.0	0.1233	2.606	0	-3.936
1.44	0.127	2.361	0	-3.806
1.85	0.1228	2.156	0	-3.745

TABLE II. Plasma Mach number and electrostatic potential for different values of  $\nu_2$  and  $\nu_1 = 0.1$ .

monotonous behavior of the plasma velocity in the outer region where the magnetic field is almost flat, between  $z/L = 0.8$  and  $z/L = 1$ , see Fig 15. The width of the region with the density increase on the left side of the mirror is also increasing with  $\nu_2$  as shown in Fig. 16. The characteristic increase in the perpendicular pressure so well pronounced for  $\nu_2 = \nu_1 = 0$ , is smoothed out by finite values of  $\nu_2$  and eventually disappears for large values of  $\nu_2$  as shown in Fig. 18. The reduction of the velocity at the exit side, is consistent with the lower overall drop in the electrostatic potential as shown in Fig. 19 and displayed in Table II.

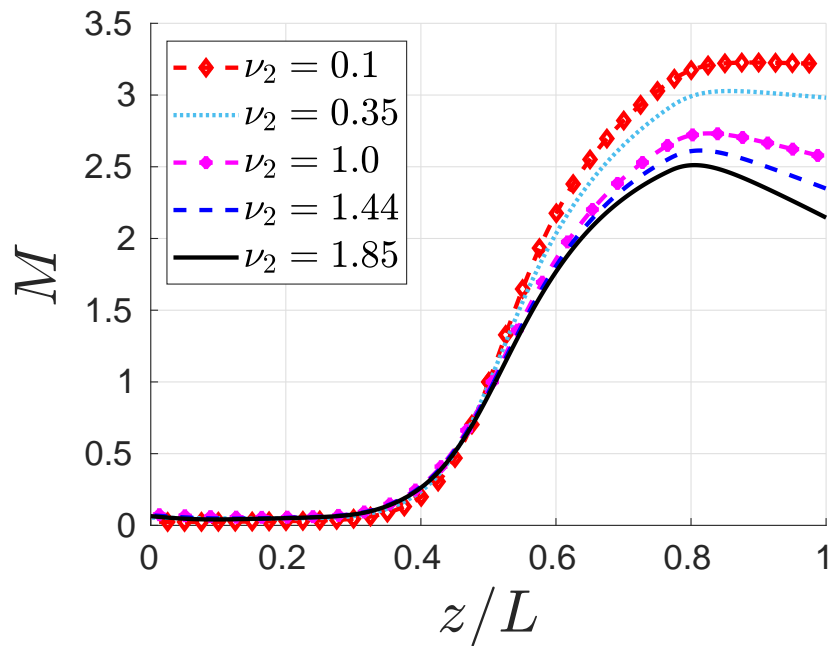


FIG. 15. Mach number  $M$  for  $\nu_1 = 0.1$  and different values of  $\nu_2$ .

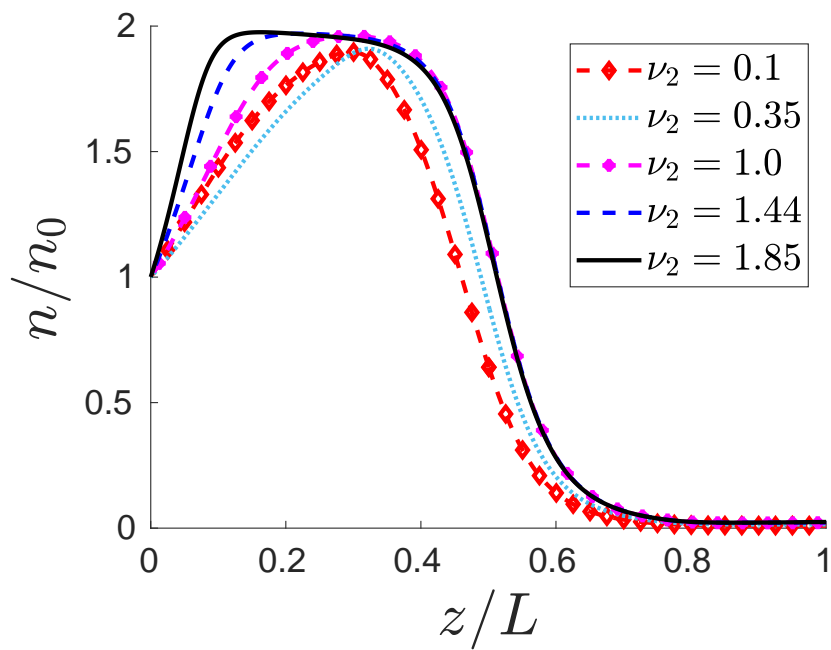


FIG. 16. Plasma density for  $\nu_1 = 0.1$  and different values of  $\nu_2$ .

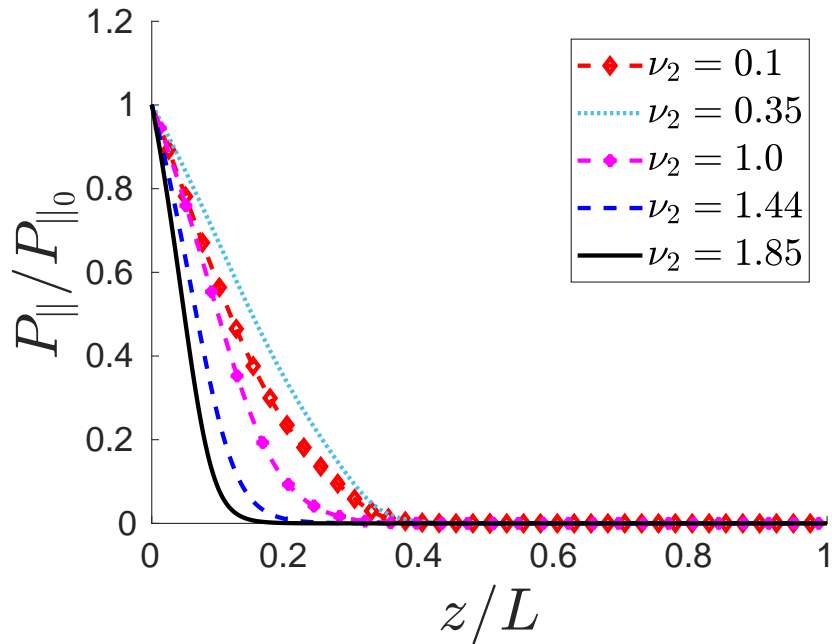


FIG. 17. Parallel pressure for  $\nu_1 = 0.1$  and different values of  $\nu_2$ .

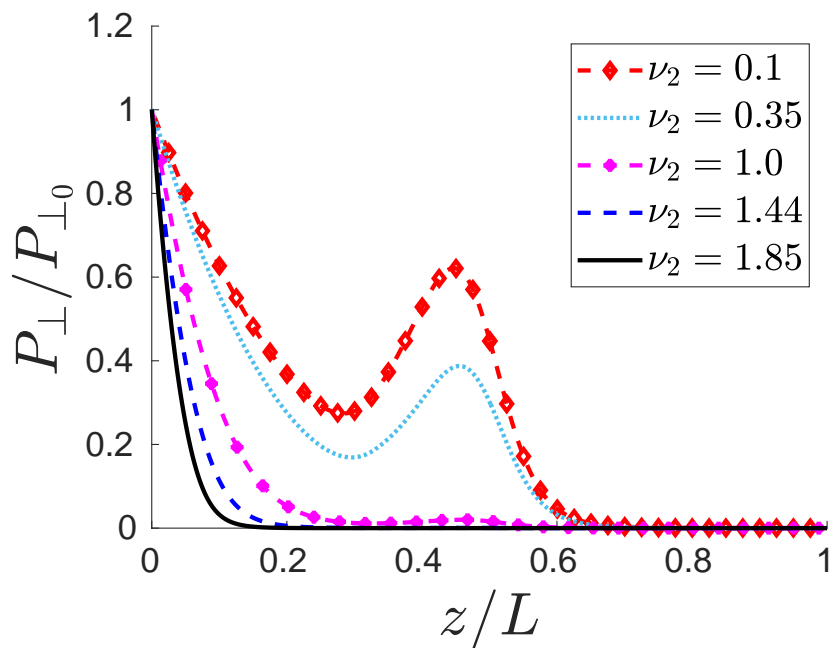


FIG. 18. Perpendicular pressure for  $\nu_1 = 0.1$  and different values of  $\nu_2$ .

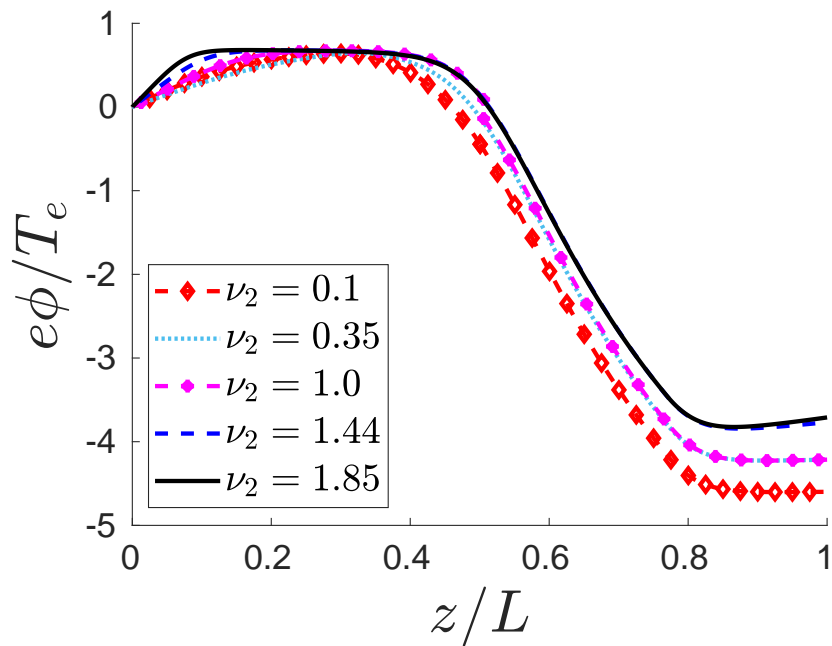


FIG. 19. Electrostatic potential for  $\nu_1 = 0.1$  and different values of  $\nu_2$ .

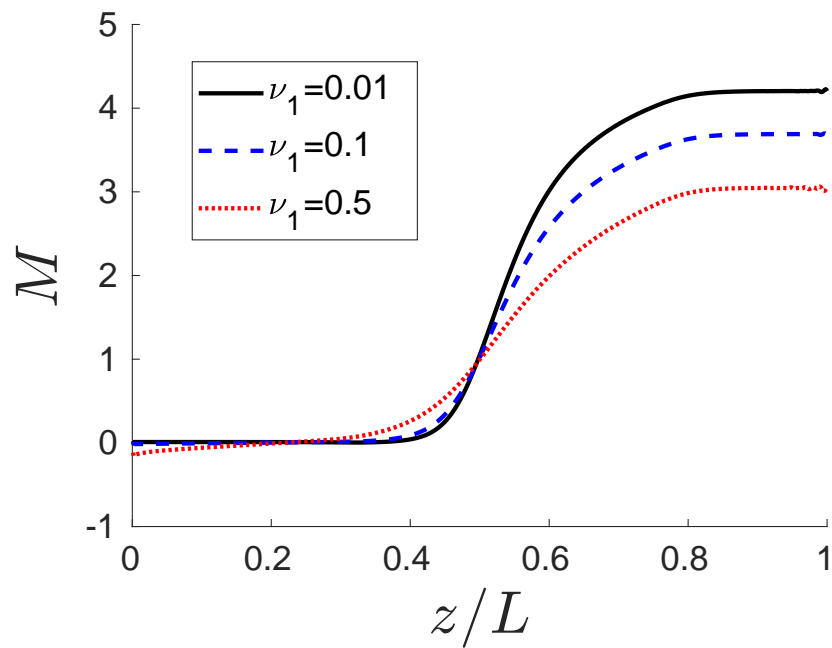


FIG. 20. Mach number for various values of  $\nu_1$  (ionization) and  $\nu_2 = 0$ .

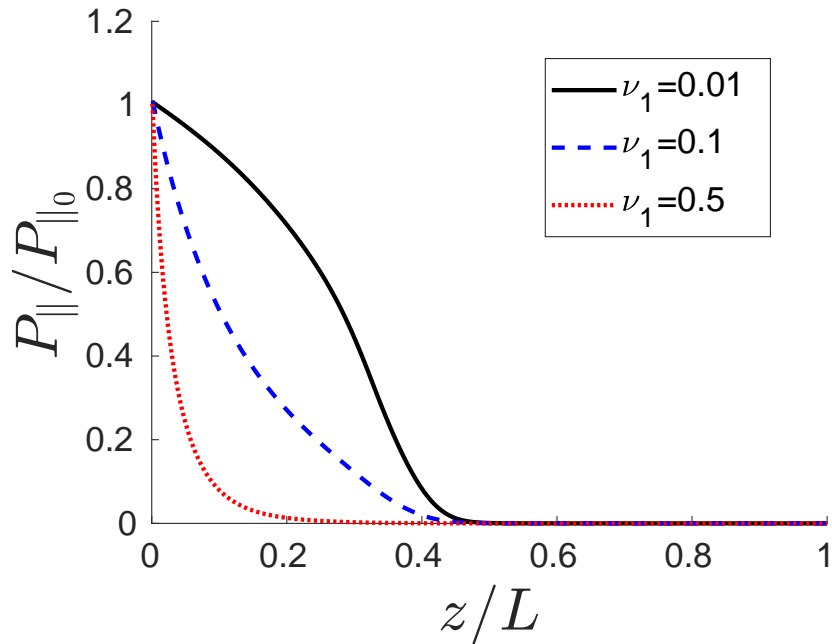


FIG. 21. Parallel pressure for various values of  $\nu_1$  (ionization) and  $\nu_2 = 0$ .

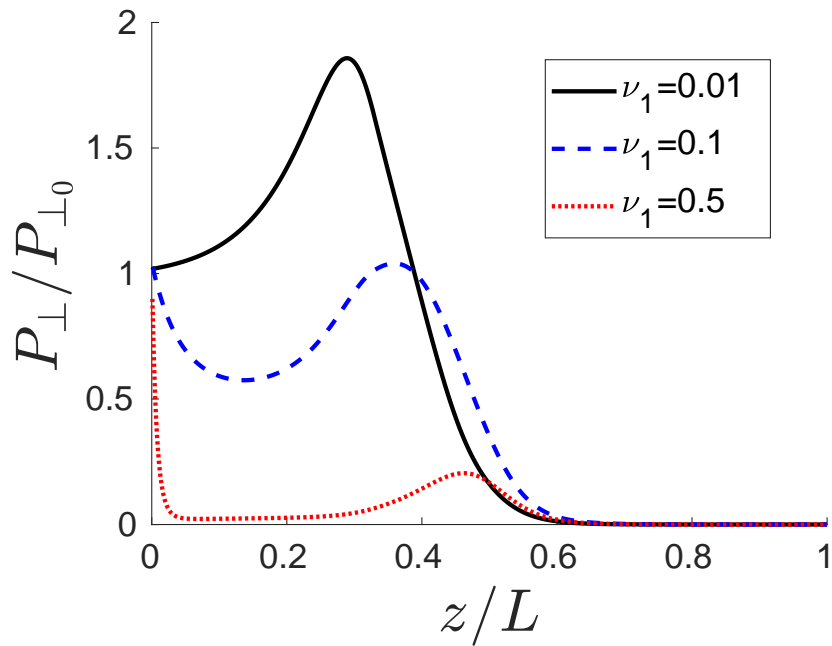


FIG. 22. Perpendicular pressure for various values of  $\nu_1$  (ionization) and  $\nu_2 = 0$ .

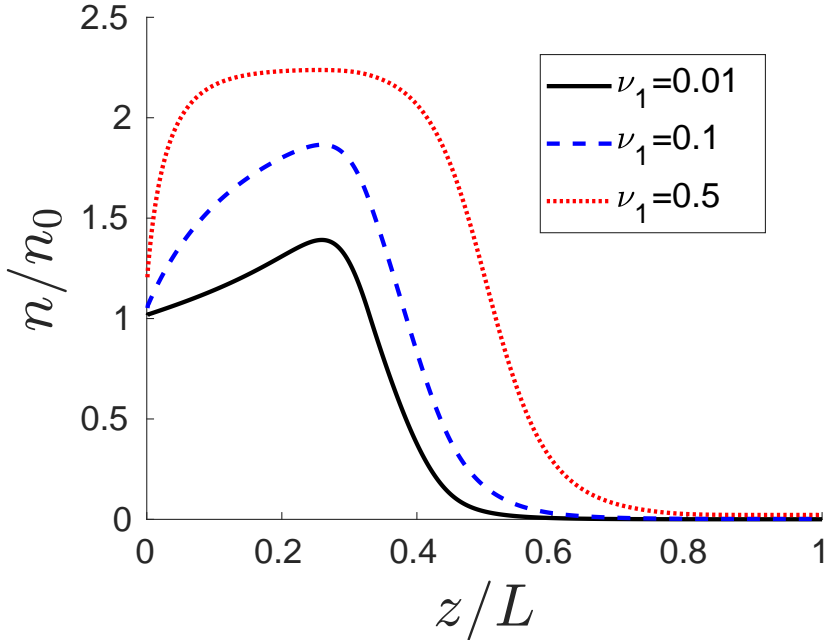


FIG. 23. Plasma density profiles for various values of  $\nu_1$  (ionization) and  $\nu_2 = 0$ .

## VII. DISCUSSION AND CONCLUSIONS

The flow of plasma in a magnetic nozzle was studied in the paraxial approximation using a two fluid MHD model with fully magnetized ions and anisotropic pressure. We have shown that within the quasineutral approximation the regularization condition at the sonic point defines the global solution for the whole region involving the magnetic mirror. This is the unique accelerating solution with  $0 < V_{\parallel} < c_s$  from the interior of the magnetic mirror with  $V_{\parallel} < c_s$  to the expander region of the divertor where the ion velocity can significantly exceed the ion sound velocity. Plasma acceleration occurs as a result of an ambipolar electrostatic potential drop formed in the magnetic mirror converting finite plasma pressure into the ion kinetic energy. It was shown that the finite perpendicular ion temperature increases the finite ion velocity in the exit region due to the effect of the mirror force. The finite (accelerated) value of the plasma velocity is defined by the electron and ion temperatures and the magnetic mirror aspect ratio.

The coupling of plasma flow with neutrals is important in many fusion<sup>3</sup> and plasma thruster applications<sup>31-33</sup>. Model equations were used to point out characteristic effects due

to ionization and charge-exchange processes. These effects shift the position of the sonic point from the maximum magnetic field as in the ideal case. Dissipation due to the ionization and charge-exchange was shown to reduce plasma acceleration and result in non-monotonous behavior of plasma density and electrostatic potential. The solutions were obtained with shooting method and were further confirmed with initial value time-dependent simulations.

Here a simplified model was used neglecting a number of important effects. Similarly to Refs. 34 and 35 our model is a paraxial approximation which considers the radial variations only in the main order. Though such one-dimensional models are often a good approximation for a full two-dimensional dynamics<sup>25</sup>, two-dimensional effects are expected to be important<sup>9</sup> for large diameter system and need to be included. Though the detachment problem may not be critical for fusion application and in presence of dissipation such as charge-exchange effects, it would need to be considered for space propulsion applications<sup>36</sup>.

In general ion kinetic effects are important for low density collisionless plasmas as in Refs. 3 and 29. One of the related limitations of the current study is the use of the simplistic two-pressure CGL model for ions. This approximation neglects the ion heat fluxes that need to be included either with extended two-pressure models and/or with full kinetic theory<sup>35,37</sup>. The neglect of ion parallel heat fluxes in our model may be the reason for the behavior of the ion parallel pressure which is fast decreasing into the mirror region in our model while the experiments do not show such behavior<sup>3</sup>. The kinetic ion model would also be required to describe the possible ion trapping and demagnetization effects for very low values of the magnetic field in the expander region. It would be interesting to implement kinetic closures<sup>21</sup> for the heat flux as proposed in Refs.19. The assumption of isothermal Boltzmann electron is another serious limitation. It is expected that the electron cooling and trapped electrons in the region of the diverging magnetic field (expander) are important<sup>34,38,39</sup>.

Though some sources (as ionization and charge-exchange) are included in this model, the plasma source region is not fully included. The obtained global solutions do not allow for arbitrary values of plasma velocity at the entrance point of the mirror region. Plasma density and pressure profiles are also rigidly fixed but allow arbitrary normalization factors. This raises interesting questions of how the plasma solutions in the source region can be matched to the mirror region at  $z = 0$ . It is likely to occur via partial particle reflections (that have to be described kinetically) so that the total plasma flux is determined by the plasma density in the source region (effectively by the deposited power to produce plasma).

These effects were not included in our model. One would need to fully include all plasma sources to match the source region with our global solution. Despite simplifications, the model studied here reveals a number of important physics effects which to our knowledge were not discussed in the literature. The insight provided by our simple model should be instrumental for understanding the experimental and simulations results, in particular, for bench-marking of numerical simulation codes.

## ACKNOWLEDGMENTS

This work was supported in part by NSERC Canada and the U.S. Air Force Office of Scientific Research FA9550-15-1-0226 and FA9550-21-1-0031. Computational resources were provided by Compute Canada. The authors thank the investors of TAE Technologies and the entire TAE Team for their support.

## DATA AVAILABILITY

Data generated in this study is available from the authors upon reasonable request.

## REFERENCES

- <sup>1</sup>Igor D. Kaganovich, Andrei Smolyakov, Yevgeny Raitses, Eduardo Ahedo, Ioannis G. Mikellides, Benjamin Jorns, Francesco Taccogna, Renaud Gueroult, Sedina Tsikata, Anne Bourdon, Jean-Pierre Boeuf, Michael Keidar, Andrew Tasman Powis, Mario Merino, Mark Cappelli, Kentaro Hara, Johan A. Carlsson, Nathaniel J. Fisch, Pascal Chabert, Irina Schweigert, Trevor Lafleur, Konstantin Matyash, Alexander V. Khrabrov, Rod W. Boswell, and Amnon Fruchtman. Physics of  $E \times B$  discharges relevant to plasma propulsion and similar technologies. *Physics of Plasmas*, 27(12):120601, 2020.
- <sup>2</sup>B. W. Longmier, E. A. Bering, M. D. Carter, L. D. Cassady, W. J. Chancery, F. R. C. Diaz, T. W. Glover, N. Hershkowitz, A. V. Ilin, G. E. McCaskill, C. S. Olsen, and J. P. Squire. Ambipolar ion acceleration in an expanding magnetic nozzle. *Plasma Sources Science & Technology*, 20(1):015007, 2011.

<sup>3</sup>M. Onofri, P. Yushmanov, S. Detrick, D. Barnes, K. Hubbard, and T. Tajima. Magnetohydrodynamic transport characterization of a field reversed configuration. *Physics of Plasmas*, 24(9):092518, 2017.

<sup>4</sup>H. Bufferand, G. Ciraolo, G. Dif-Pradalier, P. Ghendrih, P. Tamain, Y. Marandet, and E. Serre. Magnetic geometry and particle source drive of supersonic divertor regimes. *Plasma Physics and Controlled Fusion*, 56(12):122001, 2014.

<sup>5</sup>A. Kirk, W. Fundamenski, J. W. Ahn, and G. Counsell. Parallel sol transport in mast and jet: the impact of the mirror force. *Plasma Physics and Controlled Fusion*, 45(8):1445–1463, 2003.

<sup>6</sup>P. Ghendrih, K. Bodi, H. Bufferand, G. Chiavassa, G. Ciraolo, N. Fedorczak, L. Isoardi, A. Paredes, Y. Sarazin, E. Serre, F. Schwander, and P. Tamain. Transition to supersonic flows in the edge plasma. *Plasma Physics and Controlled Fusion*, 53(5):054019, 2011.

<sup>7</sup>A.I. Morozov and L.S. Solovev. Reviews of plasma physics/voprosy teorii plazmy. volume 8. Springer, Atomizdat Moscow 1974, New York, 1980.

<sup>8</sup>E. B. Hooper. Plasma detachment from a magnetic nozzle. *Journal of Propulsion and Power*, 9(5):757–763, 1993.

<sup>9</sup>E. Ahedo and M. Merino. Two-dimensional supersonic plasma acceleration in a magnetic nozzle. *Physics of Plasmas*, 17(7):073501, 2010.

<sup>10</sup>M. Merino and E. Ahedo. Fully magnetized plasma flow in a magnetic nozzle. *Physics of Plasmas*, 23(2):023506, 2016.

<sup>11</sup>M. Inutake, K. Yoshino, S. Fujimura, H. Tobari, T. Yagai, Y. Hosokawa, R. Sato, K. Hattori, and A. Ando. Production of a high-mach-number plasma flow for an advanced plasma space thruster. *Plasma Science & Technology*, 6(6):2541–2545, 2004.

<sup>12</sup>M. Inutake, A. Ando, K. Hattori, H. Tobari, T. Makita, M. Shibata, Y. Kasashima, and T. Komagome. Generation of supersonic plasma flows using an applied-field mpd arcjet and icrf heating. *Plasma Physics and Controlled Fusion*, 49(5A):A121–A134, 2007.

<sup>13</sup>Rajiv Goswami, Jean-François Artaud, Frédéric Imbeaux, and Predhiman Kaw. Numerical study of transition to supersonic flows in the edge plasma. *Physics of Plasmas*, 21(7):072510, 2014.

<sup>14</sup>S. Togo, D. Reiser, P. Borner, M. Sakamoto, N. Ezumi, and Y. Nakashima. Benchmarking of b2 code with a one-dimensional plasma fluid model incorporating anisotropic ion pressures on simple mirror configurations. *Plasma and Fusion Research*, 13:3403022, 2018.

<sup>15</sup>S. Togo, T. Takizuka, D. Reiser, M. Sakamoto, N. Ezumi, Y. Ogawa, K. Nojiri, K. Ibano, Y. Li, and Y. Nakashima. Self-consistent simulation of supersonic plasma flows in advanced divertors. *Nuclear Fusion*, 59(7):076041, 2019.

<sup>16</sup>A. I. Smolyakov, A. Sabo, P. Yushmanov, and S. Putvinskii. On quasineutral plasma flow in the magnetic nozzle. *Physics of Plasmas*, 28(6):060701, 2021.

<sup>17</sup>G. F. Chew, M. L. Goldberger, and F. E. Low. *Proc. R. Soc. London, Ser. A*, **236**:112, (1956).

<sup>18</sup>E. Zawaideh, F. Najmabadi, and R. W. Conn. *Phys. Fluids*, **29**:463, (1986).

<sup>19</sup>Zehua Guo, Xian-Zhu Tang, and Chris McDevitt. Parallel heat flux and flow acceleration in open field line plasmas with magnetic trapping. *Physics of Plasmas*, 21(10):102512, 2014.

<sup>20</sup>A. I. Smolyakov and X. Garbet. Drift kinetic equation in the moving reference frame and reduced magnetohydrodynamic equations. *Physics of Plasmas*, 17(4):042105, 2010.

<sup>21</sup>P. B. Snyder, G. W. Hammett, and W. Dorland. Landau fluid models of collisionless magnetohydrodynamics. *Physics of Plasmas*, 4(11):3974–3985, 1997.

<sup>22</sup>S. Robertson. A reduced set of gyrofluid equations for plasma flow in a diverging magnetic field. *Physics of Plasmas*, 23(4):043513, 2016.

<sup>23</sup>B. Lehnert. Rotating plasmas. *Nuclear Fusion*, 11(5):485–533, 1971.

<sup>24</sup>W. M. Manheimer and R. F. Fernsler. Plasma acceleration by area expansion. *Ieee Transactions on Plasma Science*, 29(1):75–84, 2001.

<sup>25</sup>A. Fruchtman, K. Takahashi, C. Charles, and R. W. Boswell. A magnetic nozzle calculation of the force on a plasma. *Physics of Plasmas*, 19(3):033507, 2012.

<sup>26</sup>S. Togo, T. Takizuka, D. Reiser, M. Sakamoto, Y. Ogawa, N. Ezumi, K. Ibano, K. Nojiri, Y. Li, and Y. Nakashima. Characteristics of plasma flow profiles in a super-x-divertor-like configuration. *Nuclear Materials and Energy*, 19:149–154, 2019.

<sup>27</sup>Alexander E. Dubinov and Irina D. Dubinova. How can one solve exactly some problems in plasma theory. *Journal of Plasma Physics*, 71(05):715, 2005.

<sup>28</sup>J. L. Raimbault, L. Liard, J. M. Rax, P. Chabert, A. Fruchtman, and G. Makrinich. Steady-state isothermal bounded plasma with neutral dynamics. *Physics of Plasmas*, 14(1):013503, 2007.

<sup>29</sup>M. W. Binderbauer, T. Tajima, M. Tuszewski, L. Schmitz, A. Smirnov, H. Gota, E. Garate, D. Barnes, B. H. Deng, E. Trask, X. Yang, S. Putvinski, R. Andow, N. Bolte, D. Q. Bui,

F. Ceccherini, R. Clary, A. H. Cheung, K. D. Conroy, S. A. Detrick, J. D. Douglass, P. Feng, L. Galeotti, F. Giannanco, E. Granstedt, D. Gupta, S. Gupta, A. A. Ivanov, J. S. Kinley, K. Knapp, S. Korepanov, M. Hollins, R. Magee, R. Mendoza, Y. Mok, A. Necas, S. Primavera, M. Onofri, D. Osin, N. Rath, T. Roche, J. Romero, J. H. Schroeder, L. Sevier, A. Sibley, Y. Song, L. C. Steinhauer, M. C. Thompson, A. D. Van Drie, J. K. Walters, W. Waggoner, P. Yushmanov, K. Zhai, and T. A. E. Team. Recent breakthroughs on c-2u: Norman’s legacy. In T. Tajima and M. Binderbauer, editors, *Physics of Plasma-Driven Accelerators and Accelerator-Driven Fusion*, volume 1721 of *AIP Conference Proceedings*, page 030003. 2016.

<sup>30</sup>M. Lieberman and A. Lichtenberg. *Principles of plasma discharges and materials processing*. (Wiley-Blackwell, 2005).

<sup>31</sup>A. Fruchtman. Neutral gas depletion in low temperature plasma. *Journal of Physics D-Applied Physics*, 50(47):473002, 2017.

<sup>32</sup>B. Wachs and B. Jorns. Background pressure effects on ion dynamics in a low-power magnetic nozzle thruster. *Plasma Sources Science & Technology*, 29(4):045002, 2020.

<sup>33</sup>K. Takahashi, Y. Takao, and A. Ando. Neutral-depletion-induced axially asymmetric density in a helicon source and imparted thrust. *Applied Physics Letters*, 108(7):074103, 2016.

<sup>34</sup>M. Merino, J. Maurino, and E. Ahedo. Kinetic electron model for plasma thruster plumes. *Plasma Sources Science and Technology*, 27(3):035013, 2018.

<sup>35</sup>E. Ahedo, S. Correyero, J. Navarro-Cavallé, and M. Merino. Macroscopic and parametric study of a kinetic plasma expansion in a paraxial magnetic nozzle. *Plasma Sources Science and Technology*, 29(4):045017, 2020.

<sup>36</sup>B. N. Breizman, M. R. Tushentsov, and A. V. Arefiev. Magnetic nozzle and plasma detachment model for a steady-state flow. *Physics of Plasmas*, 15(5):057103, 2008.

<sup>37</sup>Manuel Martinez-Sanchez and Eduardo Ahedo. Magnetic mirror effects on a collisionless plasma in a convergent geometry. *Physics of Plasmas*, 18(3):033509, 2011.

<sup>38</sup>B. A. Wetherton, A. Le, J. Egedal, C. Forest, W. Daughton, A. Stanier, and S. Boldyrev. A drift kinetic model for the expander region of a magnetic mirror. *Physics of Plasmas*, 28(4):042510, 2021.

<sup>39</sup>D. I. Skovorodin. Influence of trapped electrons on the plasma potential in the expander of an open trap. *Plasma Physics Reports*, 45(9):799–804, 2019.

## Appendix A: Magnetic field profile

To study the effects of finite ion temperature we employed a mirror magnetic field. To simplify numerical calculations, the magnetic field was described by three different functions in regions A, B, and C: the region A, from  $z' = z/L = 0$  to  $z' = 0.33$ , with  $B_A(z') = 0.5e^{-84(z'-0.5)^2} + B_0$ ,  $B_0 = 0.067$  (T); the region B from  $z' = 0.33$  to  $z' = 0.77$  with  $B_B(z') = B_m (0.13)^3 / ((0.13)^2 + (z' - z_m)^2)^{\frac{3}{2}}$ , where  $B_m = 0.5365(T)$  is the magnetic field at the maximum at  $z' = z_m$ ; the regions C from  $z' = 0.77$  to  $z' = 1$  with  $B_C(z') = 0.55e^{-51(z'-0.5)} + B_r$ ,  $B_r = 0.0268$  (T). The functions  $B_A(z')$ ,  $B_B(z')$ , and  $B_C(z')$  are chosen to have  $B$  and  $dB/dz$  continuous across the boundaries  $A - B$  and  $B - C$ .

## Appendix B: Time-dependent equations

The solutions of the stationary equations were verified with the initial value simulations of the time-dependent equations. In the absence of charge-exchange and ionization it has the following form:

$$\frac{\partial n}{\partial t} = nM \frac{\partial \ln B}{\partial z} - M \frac{\partial n}{\partial z} - n \frac{\partial M}{\partial z} + \alpha_1 \frac{\partial^2 n}{\partial z^2}, \quad (B1)$$

$$\frac{\partial p_{\parallel}}{\partial t} = p_{\parallel}M \frac{\partial \ln B}{\partial z} - M \frac{\partial p_{\parallel}}{\partial z} - 3p_{\parallel} \frac{\partial M}{\partial z} + \alpha_2 \frac{\partial^2 p_{\parallel}}{\partial z^2}, \quad (B2)$$

$$\frac{\partial p_{\perp}}{\partial t} = 2p_{\perp}M \frac{\partial \ln B}{\partial z} - M \frac{\partial p_{\perp}}{\partial z} - p_{\perp} \frac{\partial M}{\partial z} + \alpha_3 \frac{\partial^2 p_{\perp}}{\partial z^2}, \quad (B3)$$

$$\begin{aligned} \frac{\partial M}{\partial t} = & -M \frac{\partial M}{\partial z} - \frac{1}{n} \frac{\partial n}{\partial z} - \frac{1}{nT_e} \frac{\partial p_{\parallel}}{\partial z} + \\ & \frac{1}{nT_e} (p_{\parallel} - p_{\perp}) \frac{\partial \ln B}{\partial z} + \alpha_4 \frac{\partial^2 M}{\partial z^2}. \end{aligned} \quad (B4)$$

Here, all the quantities are expressed in dimensionless units. The diffusive coefficients  $\alpha$  had the following values:  $\alpha_1 = 5.0 \times 10^{-6}$ ,  $\alpha_2 = 5.0 \times 10^{-6}$ ,  $\alpha_3 = 5.0 \times 10^{-6}$  and  $\alpha_4 = 1.0 \times 10^{-9}$ .

The values for the diffusion coefficients  $\alpha$  were small in comparison to the other terms in the equation and thus their addition did not affect the physics of the problem. For

instance, for a value of  $\alpha = 5.0 \times 10^{-6}$ ,  $M = 3.179 \times 10^{-4}$  and  $L = 4$  the condition  $M/L = 7.95 \times 10^{-5} \gg \alpha/L^2 = 3.13 \times 10^{-7}$  holds.

When ionization and charge-exchange effects were included in the model, the time-dependent equations had the form

$$\begin{aligned} \frac{\partial n}{\partial t} = & nM \frac{\partial \ln B}{\partial z} - M \frac{\partial n}{\partial z} - n \frac{\partial M}{\partial z} + \nu_1 n \\ & + \beta_1 \frac{\partial^2 n}{\partial z^2}, \end{aligned} \quad (B5)$$

$$\begin{aligned} \frac{\partial p_{\parallel}}{\partial t} = & p_{\parallel} M \frac{\partial \ln B}{\partial z} - M \frac{\partial p_{\parallel}}{\partial z} - 3p_{\parallel} \frac{\partial M}{\partial z} - \nu_2 p_{\parallel} \\ & + \beta_2 \frac{\partial^2 p_{\parallel}}{\partial z^2}, \end{aligned} \quad (B6)$$

$$\begin{aligned} \frac{\partial p_{\perp}}{\partial t} = & 2p_{\perp} M \frac{\partial \ln B}{\partial z} - M \frac{\partial p_{\perp}}{\partial z} - p_{\perp} \frac{\partial M}{\partial z} - \nu_2 p_{\perp} \\ & + \beta_3 \frac{\partial^2 p_{\perp}}{\partial z^2}, \end{aligned} \quad (B7)$$

$$\begin{aligned} \frac{\partial M}{\partial t} = & -M \frac{\partial M}{\partial z} - \frac{1}{n} \frac{\partial n}{\partial z} - \frac{1}{nT_e} \frac{\partial p_{\parallel}}{\partial z} + \\ & \frac{1}{nT_e} (p_{\parallel} - p_{\perp}) \frac{\partial \ln B}{\partial z} - \nu_2 M + \beta_4 \frac{\partial^2 M}{\partial z^2}. \end{aligned} \quad (B8)$$

The diffusion coefficients  $\beta$  were dimensionless and had the following values:  $\beta_1 = 1.0 \times 10^{-3}$ ,  $\beta_2 = 6.0 \times 10^{-3}$ ,  $\beta_3 = 9.9 \times 10^{-4}$  and  $\beta_4 = 1.0 \times 10^{-4}$ .

Similar to the values of  $\alpha$ , the values of  $\beta$  were small and did not affect the physics of the problem. For instance for  $\beta = 1.0 \times 10^{-3}$ ,  $M = 0.127$  and  $L = 4$  the condition  $M/L = 0.032 \gg \beta/L^2 = 6.25 \times 10^{-5}$  is true and the addition of the parameters  $\beta$  did not affect the physics of the problem.

The time-dependent equations describing the flow of plasma were solved in BOUT++. In the BOUT++ simulations,  $p_{\parallel}$  was displaying oscillatory behavior in region A of the nozzle. These oscillations were damped as  $t$  increased and the time-dependent value of  $p_{\parallel}$  approached the stationary solution value.